JACS
JOURNAL OF THE AMERICAN CHEMICAL SOCIETY
pubs.acs.org/JACS
Article

Molecular Engineering of Metal–Organic Layers for Sustainable Tandem and Synergistic Photocatalysis

Yingjie Fan, Haifeng Zheng, Steven Labalme, and Wenbin Lin*

Cite This: J. Am. Chem. Soc. 2023, 145, 4158–4165
Read Online

ABSTRACT: Metal–organic layers (MOLs), a monolayered version of metal–organic frameworks (MOFs), have recently emerged as a novel two-dimensional molecular material platform to design multifunctional catalysts. MOLs inherit the intrinsic molecular tunability of MOFs and yet have more accessible and modifiable building blocks. Here we report molecular engineering of six MOLs via modulated solvothermal synthesis between $HfCl_4$ and three photosensitizing ligands followed by postsynthetic modification with two carboxylate-containing cobaloximes for tandem and synergistic photocatalysis. Morphological and structural characterization by transmission electron microscopy and atomic force microscopy and compositional analysis by inductively coupled plasma-mass spectrometry and nuclear magnetic resonance spectroscopy establish the MOLs as flat nanoplates with a periodic lattice structure of hexagonal symmetry. The MOLs efficiently catalyze tandem dehydrogenative coupling reactions and synergistic Heck-type coupling reactions. The most active MOL catalyst was used for the gram-scale synthesis of vesnarinone, a cardiotonic agent, in 80% yield with a turnover number of 400 and in eight consecutive reaction cycles without significant loss of activities.

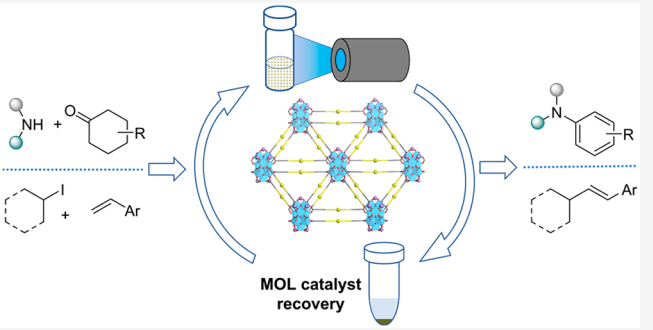

INTRODUCTION

Metal–organic frameworks (MOFs) have received broad interest in the fields of chemistry and materials science over the past three decades.[1,2] The framework stability and porosity of MOFs have enabled their applications in gas storage and separation,[3−5] drug delivery,[6] and heterogeneous catalysis.[7−13] The superiority of MOFs over other porous inorganic materials derives from the ability to control the framework structures and pore dimensions via judicious choices of secondary building units (SBUs) and bridging ligands. Well-established molecular chemistry can be introduced into the frameworks to engineer the catalytic functions of MOF materials.[14−17] However, the hindered substrate diffusion through the pores/channels of limited sizes (typically <2 nm) and the difficulty of incorporating multiple functional groups in three-dimensional (3D) MOFs have impeded their applications in fine chemical synthesis.[18−20]

These limitations of MOFs can be addressed via their dimensional reduction to form two-dimensional (2D) metal–organic layers (MOLs) (Figure 1a). In the presence of suitable modulators, the growth of coordination networks can be constrained to the lateral direction to yield 2D MOLs with a nanoplate morphology.[21,22] The active sites in 2D MOLs are completely accessible to organic substrates.[23,24] Furthermore, the capping monocarboxylate modulators in the vertical direction of the SBUs can be modified with active sites via carboxylate exchange to form multifunctional MOLs for catalytic transformations.[25] This strategy has been successfully used to design MOLs for photoredox dual catalysis. MOLs built from photosensitizing bridging ligands were modified with nickel, cobalt, and gold catalysts or Lewis acids for various photocatalytic transformations.[22,26−28] Installation of two catalytic sites in proximity in MOLs facilitates electron and mass transfer to significantly enhance their catalytic performance.

Although highly dispersible in common organic solvents, MOL catalysts can be readily recovered from reaction mixtures by simple centrifugation or filtration. MOL catalysts also exhibit enhanced stability over their homogeneous counterparts due to active site isolation, which shuts down common multimolecular catalyst deactivation pathways.[28,29] The ease of recovery and the extended catalyst lifetime enable the efficient reuse of MOL catalysts to reduce the consumption of precious resources, the generation of hazardous waste materials, and the economic costs.[30]

Received: November 26, 2022
Published: February 8, 2023

https://doi.org/10.1021/jacs.2c12599
J. Am. Chem. Soc. 2023, 145, 4158–4165

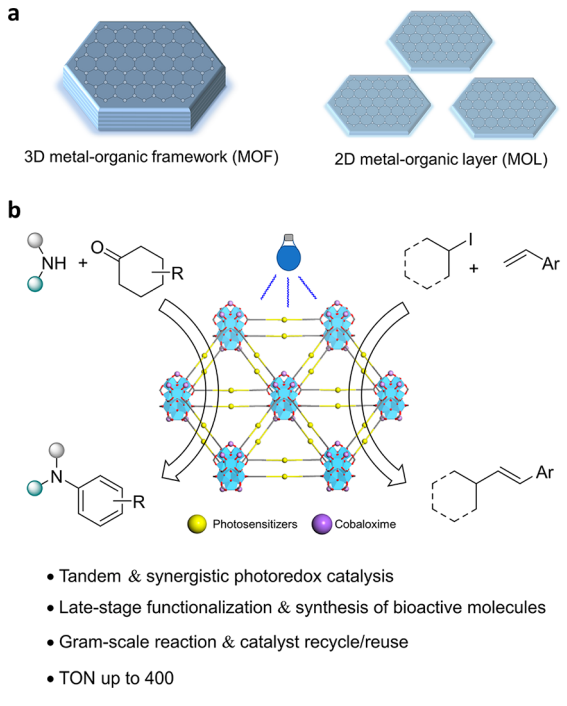

Figure 1. MOLs as a material platform for sustainable catalysis. (a) Schematic showing dimensional reduction from 3D MOFs to 2D MOLs. (b) Tandem dehydrogenative coupling reactions and synergistic Heck-type coupling reactions catalyzed by multifunctional MOLs comprising photosensitizers and cobaloximes.

Despite their great potential for sustainable catalysis, the difficulty in MOL synthesis and characterization presents a significant bottleneck for the further development of MOL catalysts. To date, only Hf_6 and H_{12} SBUs have been combined with a limited number of bridging ligands to construct MOLs.[22,24,31] Although several 2D MOFs based on Zn, Cu, and Al SBUs have been reported,[32−35] they lack stability or cannot be postsynthetically modified for catalytic applications. In recent work, a porphyrinic Hf_{12}-MOL was successfully synthesized by screening a library of monocarboxylate modulators.[24] Tuning the modulator from acetic acid to propionic acid downsized the product from a 3D MOF to a 2D MOL. Further development of synthetic methods for multifunctional MOLs should allow the design of a new generation of sustainable catalysts.

In the renaissance of visible-light-mediated photoredox chemistry, recent efforts have been devoted to organic transformations that cannot be readily accessed in a single catalytic cycle.[36,37] As an Earth-abundant element, cobalt has attracted particular attention due to its ability to mediate radical chemistry and catalyze dehydrogenative reactions.[38−49] Leonori and co-workers recently reported a tandem photochemical method for aniline synthesis from cyclohexanones and amines using cobaloximes as dehydrogenation catalysts.[50] With a wide substrate scope, this method can access and simplify the preparation of important pharmaceuticals. In another work, they discovered a halogen-atom transfer (XAT) mechanism for the activation of alkyl and aryl halides. By combining the XAT process and cobaloxime-mediated dehydrogenation, they realized synergistic Heck-type coupling reactions between alkyl iodides and aryl olefins.[51] Considering the synthetic utility of these methods, we set out to design multifunctional MOLs as sustainable catalysts to realize these transformations.

Herein, we report molecular engineering of MOLs for sustainable tandem and synergistic photoredox catalysis (Figure 1b). Hierarchical assemblies of photosensitizers (PSs) and cobaloximes in the MOLs afforded recyclable and reusable multifunctional catalysts for tandem dehydrogenative coupling reactions between amines and cyclohexanones as well as synergistic Heck-type coupling reactions between alkyl iodides and aryl olefins. A wide scope of aniline and alkene derivatives were obtained in good to excellent yields (up to 95%). The MOL catalysts were also applied to late-stage functionalization and synthesis of bioactive molecules. Gram-scale synthesis of vesnarinone, a cardiotonic agent, was achieved in 80% yield and with a turnover number (TON) of 400.

RESULTS AND DISCUSSION

Material Synthesis. A new MOL, Hf-Ir, and two known MOLs, Hf-Ru and Hf-IrF, composed of Hf_{12} SBUs and different PSs (Ir-PS, IrF-PS, Ru-PS), were synthesized via solvothermal synthesis in the presence of appropriate modulators (Figure 2a). The modulators play an essential role in MOL synthesis to produce monolayered coordination networks by suppressing the coordination of the bridging dicarboxylate ligands to the SBUs along the vertical direction. The use of dichloroacetic acid (DCA) as modulator led to the successful synthesis of a Hf-Ir MOL which was inaccessible by previous methods using trifluoracetic acid (TFA) or acetic acid.[52] Hf-IrF and Hf-Ru were also successfully synthesized using TFA as modulator. In the proposed structural model of the MOLs, each Hf_{12} SBU is laterally connected to 12 bidentate ligands to form a double-decker structure. The six remaining coordination sites on the top and bottom of each SBU are capped by monocarboxylate modulators (Figure S29). DCA and TFA modulators could be replaced by more basic carboxylates to install transition metal catalysts. By using this postsynthetic modification strategy, Hf-Ir, Hf-IrF, and Hf-Ru were further modified with two carboxylate-containing cobaloxime catalysts, Co-PPA and Co-PAPA, to yield six MOLs, Hf-Ir-Co-PPA, Hf-Ir-Co-PAPA, Hf-IrF-Co-PPA, Hf-IrF-Co-PAPA, Hf-Ru-Co-PPA, and Hf-Ru-Co-PAPA (Figure 2a).

Material Characterization. Transmission electron microscopy (TEM), high-resolution TEM (HRTEM), and fast Fourier transform (FFT) of HRTEM images revealed Hf-Ir-Co-PPA as flat nanoplates with a diameter of approximate 200 nm and a periodic lattice structure of hexagonal symmetry (Figure 2b,c). The thickness of the nanoplates was measured by atomic force microscopy (AFM) to be approximately 2.2 nm (Figure 2d), slightly higher than the height of the Hf_{12} cluster (1.7 nm) in the proposed monolayer structure. The height difference was attributed to the SBU-bound cobaloxime complexes that were introduced by replacing the smaller DCA. Hf-Ir and Hf-Ir-Co-PPA showed powder X-ray diffraction (PXRD) patterns similar to simulated and experimental PXRD patterns for a Hf-Ir MOL (Figure 2e). Extended X-ray absorption fine structure (EXAFS) analysis of Hf-Ir-Co-PPA revealed that the coordination environments of Ir and Co in the MOL were similar to those of $Ir(ppy)_2(bpy)$ and chloro(pyridine)cobaloxime, respectively, indicating that the structures of the molecular PS ligand and cobaloxime catalyst

https://doi.org/10.1021/jacs.2c12599
J. Am. Chem. Soc. 2023, 145, 4158−4165

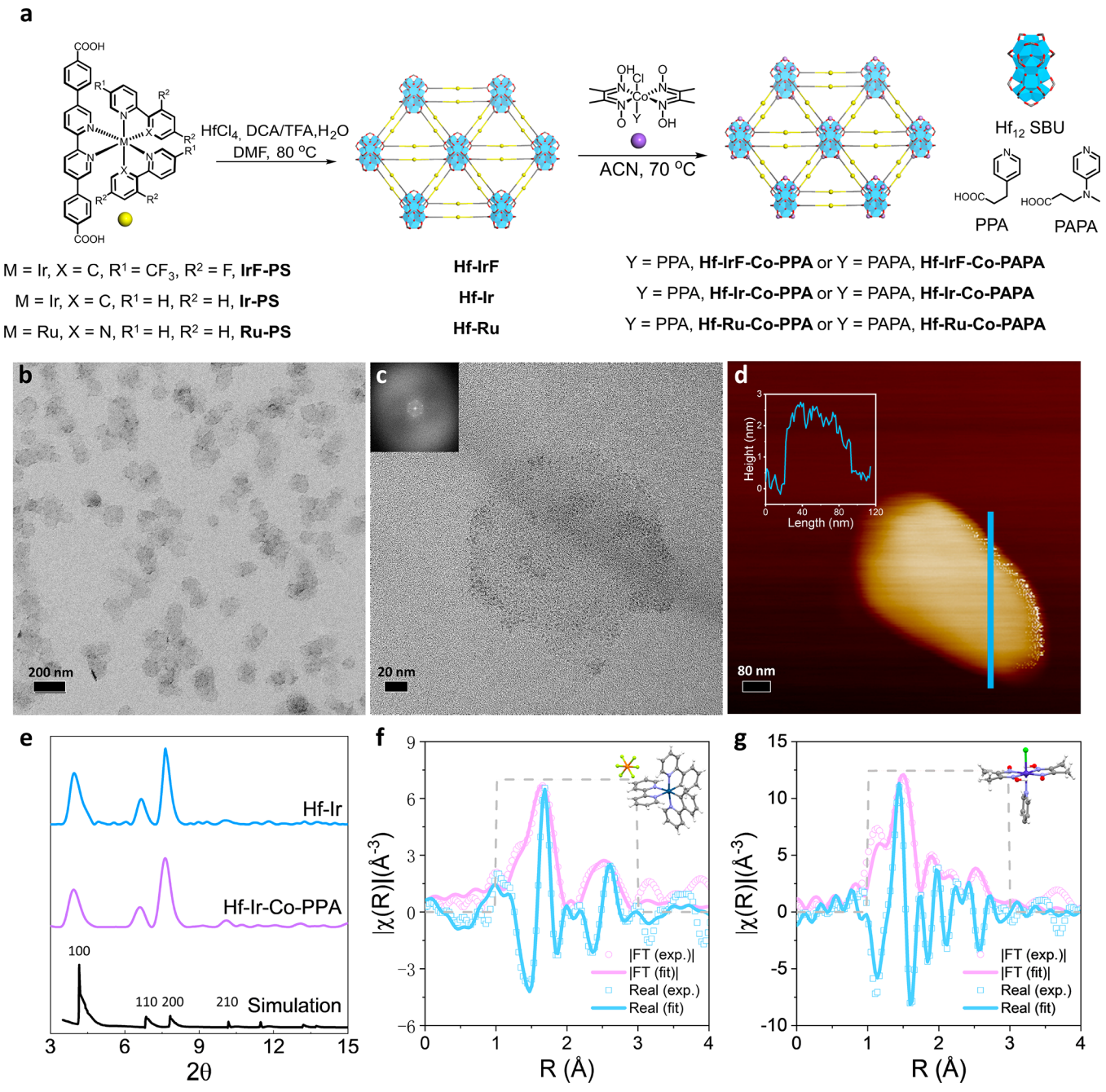

Figure 2. (a) Synthesis of MOLs. Hf-Ir, Hf-IrF, and Hf-Ru were synthesized by solvothermal reactions between $HfCl_4$ and corresponding photosensitizing dicarboxylate ligands (Ir-PS, IrF-PS, and Ru-PS), modulators (TFA or DCA), and water in *N*,*N*-dimethylformamide (DMF). Capping modulators in the MOLs were substituted by carboxylate-containing cobaloximes (Co-PPA and Co-PAPA) via postsynthetic modification to yield six MOLs, Hf-Ir-Co-PPA, Hf-Ir-Co-PAPA, Hf-IrF-Co-PPA, Hf-IrF-Co-PAPA, Hf-Ru-Co-PPA, and Hf-Ru-Co-PAPA. Characterization of Hf-Ir-Co-PPA. (b) TEM image of Hf-Ir-Co-PPA. (c) HRTEM image of Hf-Ir-Co-PPA. FFT pattern is shown in the inset. (d) AFM image of Hf-Ir-Co-PPA. The height profile is shown in the inset. (e) PXRD patterns of Hf-Ir and Hf-Ir-Co-PPA and simulated PXRD pattern of Hf-Ir. Miller indices are shown for the corresponding peaks in the simulated PXRD pattern. (f) EXAFS analysis of Ir in Hf-Ir-Co-PPA. The structure of the fitting model, $Ir(ppy)_2(bpy)$, is shown in the inset. (g) EXAFS analysis of Co in Hf-Ir-Co-PPA. The structure of the fitting model, $Co(dmgh)_2(Py)Cl$, is shown in the inset.

remained intact during the assembly of the Hf-Ir-Co-PPA MOL (Figure 2f,g).

Inductively coupled plasma−mass spectrometry (ICP-MS) showed that Hf-Ir-Co-PPA had a Hf:Ir:Co molar ratio of 1:0.54:0.40 (Table S2), suggesting an empirical formula of $Hf_{12}(\mu_3\text{-}O)_8(\mu_3\text{-}OH)_8(\mu_2\text{-}OH)_6(Ir\text{-}PS)_{6.5}(Co\text{-}PPA)_{4.8}(DCA)_{0.7}$. The slightly higher Ir-PS to Hf ratio of 6.5:12 than the theoretical ratio of 6:12 for the infinite 2D structure suggests that the MOL of 200 nm in dimensions was terminated by the Ir-PS ligands on the edges. This formulation was supported by proton nuclear magnetic resonance (^1H NMR) analysis of the digested Hf-Ir-Co-PPA, which showed a Co-PPA to Ir-PS molar ratio of 0.76:1 (Figure S15).

TEM, HRTEM, and AFM studies revealed that Hf-Ir-Co-PAPA, Hf-IrF-Co-PPA, Hf-IrF-Co-PAPA, Hf-Ru-Co-PPA, and Hf-Ru-Co-PAPA exhibited similar nanoplate morphologies to

https://doi.org/10.1021/jacs.2c12599
J. Am. Chem. Soc. 2023, 145, 4158−4165

Hf-Ir-Co-PPA (Figures S24–S28). As expected, the morphologies of these cobaloxime-modified MOLs were identical to the unmodified Hf-Ir, Hf-IrF, and Hf-Ru MOLs (Figure S14). ICP-MS and ^{1}H NMR analyses of the digested MOLs showed similar compositions to Hf-Ir-Co-PPA with comparable loadings of PSs and cobaloximes (Table S2). These results indicate that all six cobaloxime-modified MOLs exhibit hexagonal nanoplate morphologies based on the proposed Hf_{12} monolayer structure of kgd topology. The structures of the MOLs remained intact after postsynthetic functionalization of cobaloximes with cobaloxime loadings ranging from 60% to 80 mol % relative to the amounts of PSs.

Reaction Optimization and Mechanistic Insights. Owing to the presence of both PSs and cobaloximes, the MOLs were evaluated as catalysts for tandem dehydrogenative coupling reaction between morpholine **1a** and 4-methyl cyclohexanone **2a**. In the initial screening of reaction conditions,[50] the six MOLs showed different catalytic activities (Figure 3a). The MOLs containing Ru-PS did not catalyze the reaction. The MOLs containing Ir-PS and IrF-PS successfully catalyzed the reaction to give the aniline product **3a**. Among them, Hf-Ir-Co-PPA afforded the highest yield of 42%. Further optimization of Brønsted acids identified bistriflimidic acid ($HNTf_2$)[53] as the best acid cocatalyst to afford **3a** in a 75% isolated yield. Hf-Ir-Co-PPA outperformed its homogeneous counterpart by 7.6 times (Table S7).

According to the proposed mechanism in the literature (Figure 3b),[50] amine **1a** and cyclohexanone **2a** first condense to form an enamine. The enamine (E° = 0.26 V vs Fc^+/Fc) is then oxidized by excited PSs and deprotonates to generate a β-enamine radical, **rad**, which binds cobaloxime and undergoes a β-hydride elimination to afford the intermediate product, **int**, which proceeds through a tandem oxidation–dehydrogenation process to give the final aniline product. However, as Ir-PS, IrF-PS, and Ru-PS are strong photo-oxidants, they can competitively oxidize the amine (E° = 0.75 V vs Fc^+/Fc) to enter unproductive pathways.

Cyclic voltammetry (CV) and luminescence studies indicated that the different catalytic activities of the MOLs in the dehydrogenative coupling reactions likely resulted from the different photoredox properties of the PSs. The reduction potentials of the triplet photoexcited PSs were calculated from their emission spectra (Figure S35) and ground state reduction potentials (Figures S33, S34) to be 0.63, 0.99, and 0.61 V versus Fc^+/Fc for Ir-PS*, IrF-PS*, and Ru-PS*, respectively. Kinetic constants of photooxidation of the enamine and the amine were calculated based on the Stern–Völmer plots from luminescence quenching experiments (Figure 3c,d, Figure S36). Ir-PS* had a mildly oxidizing triplet state that was selectively quenched by the enamine. IrF-PS* had a triplet state with the strongest oxidation power and was rapidly quenched by both the enamine and the amine. Despite a low reduction potential, the triplet photoexcited Ru-PS* could still be quenched by both the enamine and the amine. The selectivities of enamine photo-oxidation over amine photo-oxidation were determined as 1068, 23, and 35 for Ir-PS, IrF-PS, and Ru-PS, respectively. Therefore, we propose that Hf-Ir-Co-PPA and Hf-Ir-Co-PAPA MOLs with Ir-PS can preferentially oxidize the enamine in the reactions to minimize side reactions and increase the product yield. The optimized strong acid catalyst $HNTf_2$ likely also improved the selectivity by accelerating the condensation reaction between cyclohexanone and morpholine to increase the enamine concentration in the

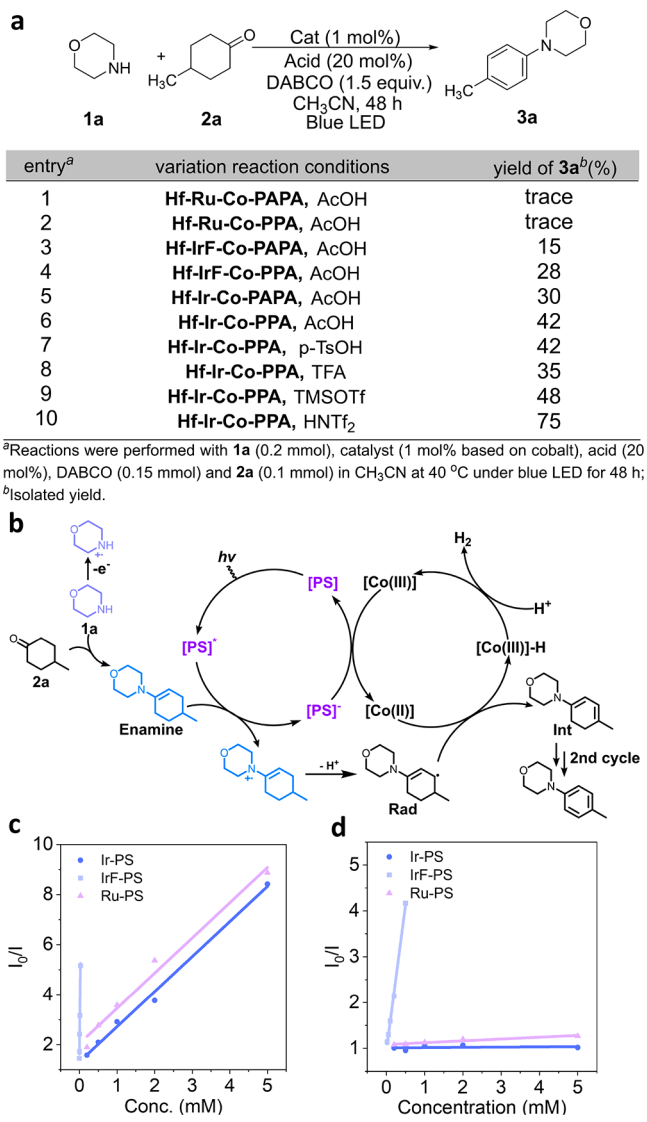

entry[a]	variation reaction conditions	yield of **3a**[b](%)
1	**Hf-Ru-Co-PAPA**, AcOH	trace
2	**Hf-Ru-Co-PPA**, AcOH	trace
3	**Hf-IrF-Co-PAPA**, AcOH	15
4	**Hf-IrF-Co-PPA**, AcOH	28
5	**Hf-Ir-Co-PAPA**, AcOH	30
6	**Hf-Ir-Co-PPA**, AcOH	42
7	**Hf-Ir-Co-PPA**, p-TsOH	42
8	**Hf-Ir-Co-PPA**, TFA	35
9	**Hf-Ir-Co-PPA**, TMSOTf	48
10	**Hf-Ir-Co-PPA**, $HNTf_2$	75

[a]Reactions were performed with **1a** (0.2 mmol), catalyst (1 mol% based on cobalt), acid (20 mol%), DABCO (0.15 mmol) and **2a** (0.1 mmol) in CH_3CN at 40 °C under blue LED for 48 h; [b]Isolated yield.

Figure 3. Reaction optimization and mechanistic studies of tandem dehydrogenative coupling reactions. (a) Reaction optimization table. (b) Proposed catalytic cycles. (c) Stern–Völmer plots of quenching studies of photoexcited PSs by 4-(4-methylcyclohex-1-en-1-yl)-morpholine (the enamine). (d) Stern–Völmer plots from quenching studies of photoexcited PSs by morpholine (the amine).

solution. Furthermore, the counteranion NTf_2^- is a weak nucleophile and does not deactivate the MOL through coordination to the SBU.

The MOLs also competently catalyzed Heck-type coupling reactions between alkyl iodides and alkenes to afford the cross-coupling products. Catalyst screening studies identified Hf-Ir-Co-PPA as the best catalyst (Table S6). Further optimization of base and alkene equivalents improved the reaction yield to 92% (Table S6). Hf-Ir-Co-PPA outperformed its homogeneous counterpart by 178 times (Table S7).

Substrate Scopes. We next investigated the substrate scopes of both amine and cyclohexanone partners in photocatalytic dehydrogenative coupling reactions under the optimized reaction conditions (Figure 4a). Secondary amines, including morpholine and protected piperidines, were suitable for these reactions, with the corresponding products **3a–3c** isolated in 58–75% yields. Primary amines, such as cyclobutyl amine, *trans*-4-methylcyclohexylamine, and (*S*)-(−)-2-amino-

https://doi.org/10.1021/jacs.2c12599
J. Am. Chem. Soc. 2023, 145, 4158–4165

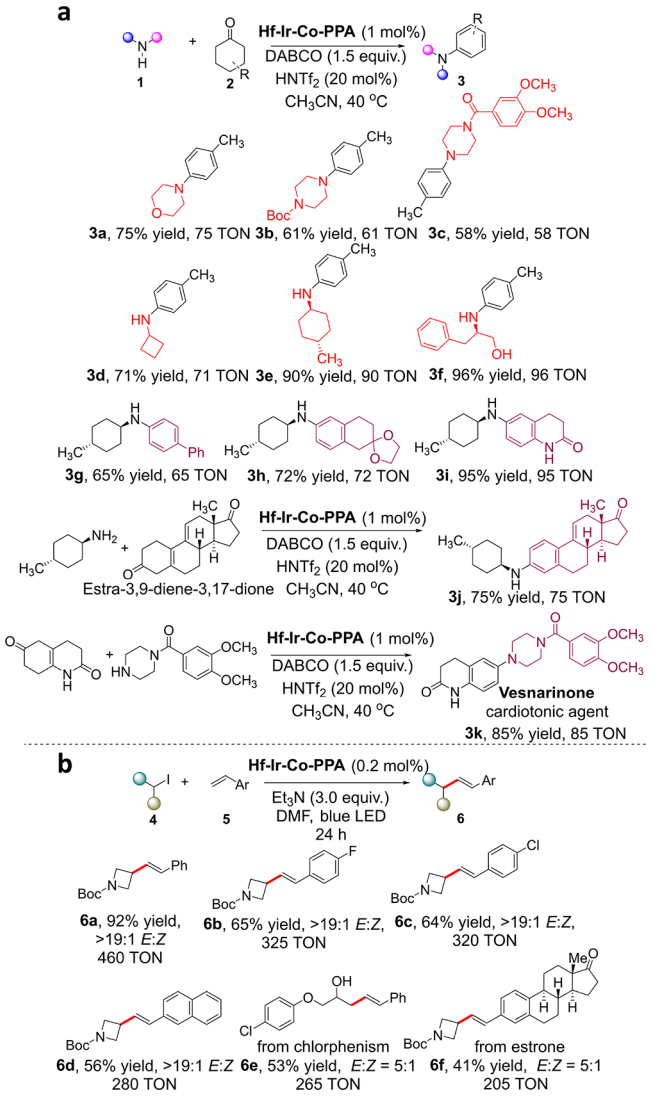

Figure 4. Substrate scopes. (a) Substrate scope of tandem dehydrogenative coupling reactions catalyzed by Hf-Ir-Co-PPA. (b) Substrate scope of synergistic Heck-type coupling reactions catalyzed by Hf-Ir-Co-PPA. TONs were calculated based on the cobaloxime catalyst for both reactions.

3-phenyl-1-propanol, smoothly reacted with 4-methyl cyclohexanone to afford products **3d**, **3e**, and **3f** in 71%, 90%, and 95% isolated yields, respectively. Mono- and disubstituted ketones were synthesized and used as substrates in the reactions to afford the desired cross-coupling products **3g**−**3i** in 65−95% isolated yields.

Hf-Ir-Co-PPA was also used for late-stage functionalization and synthesis of bioactive molecules. Improved substrate accessibility of 2D MOLs compared to 3D MOFs allows the use of large molecules as substrates in photocatalytic dehydrogenative coupling reactions. Estra-3,9-diene-3,17-dione, approximately 1.2 nm in size, efficiently underwent dehydrogenative cross-coupling reaction with *trans*-4-methylcyclohexylamine to produce the aniline product **3j** in 75% isolated yield. Vesnarinone **3k**, a cardiotonic agent of approximately 1.7 nm in size, was successfully synthesized in an 85% isolated yield by photocatalytic dehydrogenative coupling between 1,3,4,5,7,8-hexahydroquinoline-2,6-dione and (3,4-dimethoxyphenyl)(piperazin-1-yl)methanone.

Hf-Ir-Co-PPA also efficiently catalyzed Heck-type coupling reactions between alkyl iodides **4** and aryl alkenes **5**, to produce the cross-coupling products **6a**−**6f** with TONs of up to 460 (Figure 4b). Aryl alkenes bearing electron-withdrawing or electron-donating groups underwent Heck-type coupling with *tert*-butyl 3-iodoazetidine-1-carboxylate **4a** smoothly to give corresponding products **6a**−**6d** in good to excellent isolated yields. The alkyl iodide derived from the natural product chlorphenesin underwent the coupling reaction with styrene to afford **6e** in 53% isolated yield with a 5:1 *E*:*Z* ratio. The alkene derivative from the natural product estrone was also tolerated in the Heck-type coupling reaction to give **6f** in 41% isolated yield with a 5:1 *E*:*Z* ratio.

Gram-Scale Synthesis and Recycle Experiments. Gram-scale synthesis of **3k** was performed to illustrate the synthetic utility of MOL catalysts (Figure 5a). A 4 mmol amount of 1,3,4,5,7,8-hexahydroquinoline-2,6-dione and 6 mmol of (3,4-dimethoxyphenyl)(piperazin-1-yl)methanone were subjected to the standard photocatalytic dehydrogenative coupling reaction condition in the presence of 0.2 mol % Hf-Ir-Co-PPA. A 1.26 g amount of the target product, vesnarinone, was isolated as a white crystalline solid in 80% yield in 48 h. The TON of the MOL catalyst reached 400 in this one-pot synthesis.

To probe the stability of Hf-Ir-Co-PPA in the photocatalytic reaction, the catalyst was separated from the reaction mixture of the gram-scale synthesis by centrifugation. The recovered Hf-Ir-Co-PPA was washed with DMF and ethanol and examined by TEM and PXRD. TEM images showed that Hf-Ir-Co-PPA maintained the nanoplate morphology after the photocatalytic reaction (Figure 5b), whereas PXRD studies showed that the recovered Hf-Ir-Co-PPA retained the crystalline structure of as-synthesized Hf-Ir-Co-PPA (Figure 5c). These results indicate that the structure of Hf-Ir-Co-PPA remains intact during the 48 h photocatalytic reaction.

The recovered Hf-Ir-Co-PPA was then reused to catalyze the photocatalytic dehydrogenative coupling reaction. Hf-Ir-Co-PPA-catalyzed synthesis of vesnarionone was performed in a 0.1 mmol scale in eight consecutive reaction cycles. At the completion of each cycle, the MOL was collected by centrifugation, washed with acetonitrile, and directly used in the next cycle. The reaction yield gradually decreased from 85% to 76% in seven consecutive 24 h reaction cycles (Figure 5d), likely due to incomplete recovery of Hf-Ir-Co-PPA from the reaction mixture. By extending the reaction time to 36 h, the product yield returned to 82% in the eighth run. A total turnover number of 651 was achieved in the eight reaction cycles. The recyclability and stability of Hf-Ir-Co-PPA underscore the potential of MOL catalysts in sustainable photoredox catalysis.

CONCLUSIONS

We present in this work molecular engineering of multifunctional MOLs of approximately 2 nm in thickness and 200 nm in width for sustainable tandem and synergistic photocatalysis. We successfully synthesized three photosensitizing MOLs via judicious choices of monocarboxylic acid modulators and postsynthetically modified these MOLs with two cobaloxime catalysts to create a library of six MOLs for photoredox dual cobalt catalysis. Screening of these MOLs identified Hf-Ir-Co-PPA as the best catalyst for both tandem dehydrogenative coupling reactions and synergistic Heck-type coupling reactions. Hf-Ir-Co-PPA efficiently catalyzed both cross-

https://doi.org/10.1021/jacs.2c12599
J. Am. Chem. Soc. 2023, 145, 4158−4165

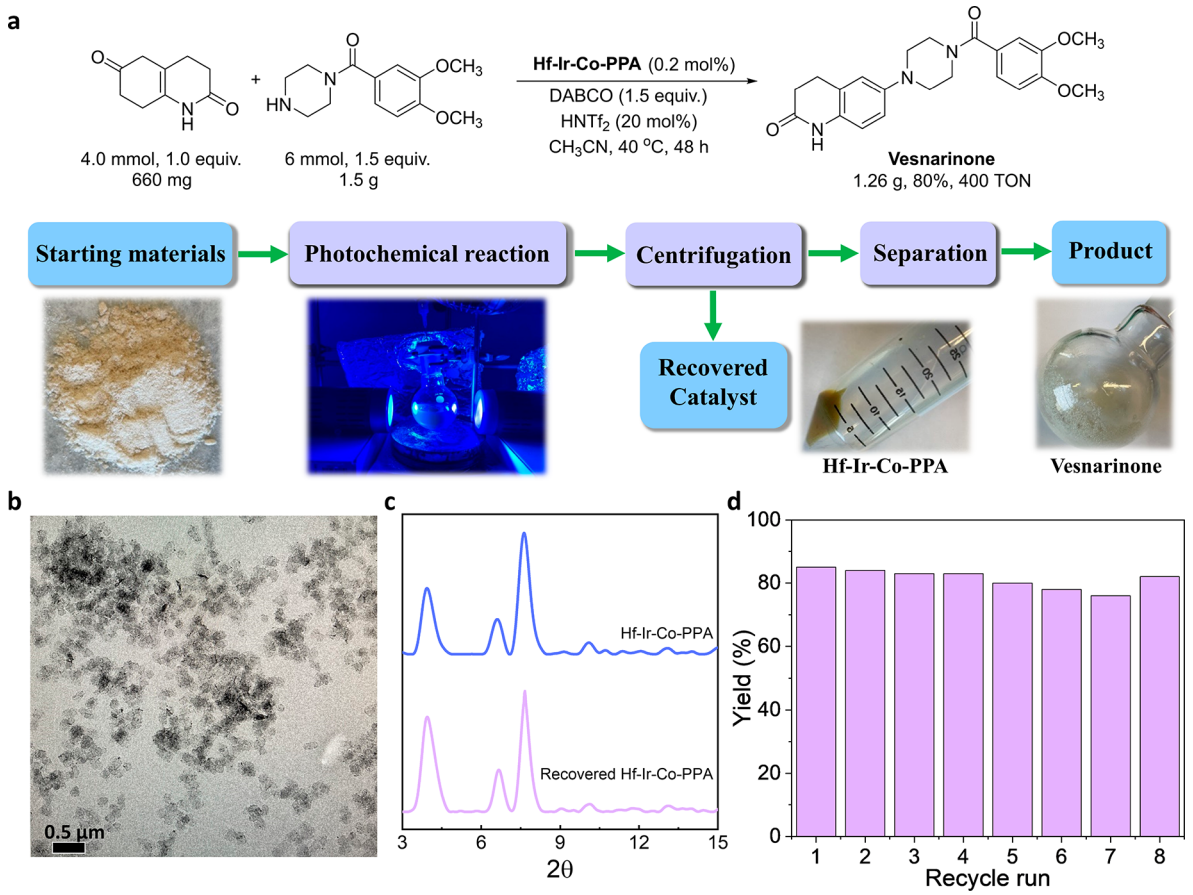

Figure 5. Gram-scale synthesis of vesnarinone and recycle experiments. (a) The protocols for Hf-Ir-Co-PPA-catalyzed gram-scale synthesis of vesnarinone and catalyst recycle. (b) TEM image of recovered Hf-Ir-Co-PPA. (c) PXRD patterns of Hf-Ir-Co-PPA before and after the photocatalytic reaction. (d) Reaction yields in eight consecutive cycles of Hf-Ir-Co-PPA-catalyzed vesnarione synthesis (0.1 mmol scale).

coupling reactions with broad substrate scopes. Owing to the hierarchical integration of both PSs and cobaloximes, the MOLs significantly outperformed their homogeneous controls with up to 178 times higher efficiency. Furthermore, Hf-Ir-Co-PPA effectively catalyzed late-stage functionalization and synthesis of large bioactive molecules owing to facile substrate accessibility to the active sites in the MOL. The synthetic utility of the MOL catalyst was also demonstrated in a one-pot gram-scale synthesis of a cardiotonic agent, vesnarinone, and by the ability to reuse the MOL in eight consecutive cycles of vesnarinone synthesis without significant loss of activity. This work highlights the potential of MOLs as a unique 2D material platform for the molecular engineering of recyclable and reusable multifunctional catalysts for sustainable tandem and synergistic photocatalysis.

■ ASSOCIATED CONTENT

Supporting Information

The Supporting Information is available free of charge at https://pubs.acs.org/doi/10.1021/jacs.2c12599.

Experimental procedures and characterization data (PDF)

Accession Codes

CCDC 2181761 contains the supplementary crystallographic data for this paper. These data can be obtained free of charge via www.ccdc.cam.ac.uk/data_request/cif, or by emailing data_request@ccdc.cam.ac.uk, or by contacting The Cambridge Crystallographic Data Centre, 12 Union Road, Cambridge CB2 1EZ, UK; fax: +44 1223 336033.

■ AUTHOR INFORMATION

Corresponding Author

Wenbin Lin − *Department of Chemistry, The University of Chicago, Chicago, Illinois 60637, United States;* orcid.org/0000-0001-7035-7759; Email: wenbinlin@uchicago.edu

Authors

Yingjie Fan − *Department of Chemistry, The University of Chicago, Chicago, Illinois 60637, United States;* orcid.org/0000-0003-1857-5788

Haifeng Zheng − *Department of Chemistry, The University of Chicago, Chicago, Illinois 60637, United States*

Steven Labalme − *Department of Chemistry, The University of Chicago, Chicago, Illinois 60637, United States*

Complete contact information is available at: https://pubs.acs.org/10.1021/jacs.2c12599

Author Contributions

Y.F. and H.Z. contributed equally to this work.

Notes

The authors declare no competing financial interest.

https://doi.org/10.1021/jacs.2c12599
J. Am. Chem. Soc. 2023, 145, 4158−4165

■ ACKNOWLEDGMENTS

We thank Sophie Whitmeyer for help with single-crystal X-ray diffraction data collection. We thank Xiaomin Jiang for his experimental help. We acknowledge the National Science Foundation (CHE-2102554) and the University of Chicago for funding support and the MRSEC Shared User Facilities at the University of Chicago (DMR-1420709) for instrument access. XAS analysis was performed at Beamline 10-BM, supported by the Materials Research Collaborative Access Team (MRCAT). Use of the Advanced Photon Source, an Office of Science User Facility operated for the U.S. DOE Office of Science by ANL, was supported by the U.S. DOE under Contract DE-AC02-06CH11357.

■ REFERENCES

(1) Yaghi, O. M.; Li, G.; Li, H. Selective binding and removal of guests in a microporous metal−organic framework. *Nature* **1995**, *378* (6558), 703−706.
(2) Furukawa, H.; Cordova, E.; O'Keeffe, M.; Yaghi Omar, M. The Chemistry and Applications of Metal-Organic Frameworks. *Science* **2013**, *341* (6149), 1230444.
(3) Li, J.-R.; Sculley, J.; Zhou, H.-C. Metal−Organic Frameworks for Separations. *Chem. Rev.* **2012**, *112* (2), 869−932.
(4) Sumida, K.; Rogow, D. L.; Mason, J. A.; McDonald, T. M.; Bloch, E. D.; Herm, Z. R.; Bae, T.-H.; Long, J. R. Carbon Dioxide Capture in Metal−Organic Frameworks. *Chem. Rev.* **2012**, *112* (2), 724−781.
(5) Zeng, H.; Xie, M.; Wang, T.; Wei, R.-J.; Xie, X.-J.; Zhao, Y.; Lu, W.; Li, D. Orthogonal-array dynamic molecular sieving of propylene/propane mixtures. *Nature* **2021**, *595* (7868), 542−548.
(6) Della Rocca, J.; Liu, D.; Lin, W. Nanoscale Metal−Organic Frameworks for Biomedical Imaging and Drug Delivery. *Acc. Chem. Res.* **2011**, *44* (10), 957−968.
(7) Lee, J.; Farha, O. K.; Roberts, J.; Scheidt, K. A.; Nguyen, S. T.; Hupp, J. T. Metal−organic framework materials as catalysts. *Chem. Soc. Rev.* **2009**, *38* (5), 1450−1459.
(8) Yi, J.-D.; Xu, R.; Wu, Q.; Zhang, T.; Zang, K.-T.; Luo, J.; Liang, Y.-L.; Huang, Y.-B.; Cao, R. Atomically Dispersed Iron−Nitrogen Active Sites within Porphyrinic Triazine-Based Frameworks for Oxygen Reduction Reaction in Both Alkaline and Acidic Media. *ACS Energy Letters* **2018**, *3* (4), 883−889.
(9) Liang, J.; Huang, Y.-B.; Cao, R. Metal−organic frameworks and porous organic polymers for sustainable fixation of carbon dioxide into cyclic carbonates. *Coord. Chem. Rev.* **2019**, *378*, 32−65.
(10) An, B.; Li, Z.; Wang, Z.; Zeng, X.; Han, X.; Cheng, Y.; Sheveleva, A. M.; Zhang, Z.; Tuna, F.; McInnes, E. J. L.; Frogley, M. D.; Ramirez-Cuesta, A. J.; Natrajan, L.; Wang, C.; Lin, W.; Yang, S.; Schröder, M. Direct photo-oxidation of methane to methanol over a mono-iron hydroxyl site. *Nat. Mater.* **2022**, *21* (8), 932−938.
(11) Wu, Z.; Li, Y.; Zhang, C.; Huang, X.; Peng, B.; Wang, G. Recent advances in metal-organic-framework-based catalysts for thermocatalytic selective oxidation of organic substances. *Chem. Catalysis* **2022**, *2* (5), 1009−1045.
(12) Lu, G.; Chu, F.; Huang, X.; Li, Y.; Liang, K.; Wang, G. Recent advances in Metal-Organic Frameworks-based materials for photocatalytic selective oxidation. *Coord. Chem. Rev.* **2022**, *450*, 214240.
(13) Xue, Y.; Zhao, G.; Yang, R.; Chu, F.; Chen, J.; Wang, L.; Huang, X. 2D metal−organic framework-based materials for electrocatalytic, photocatalytic and thermocatalytic applications. *Nanoscale* **2021**, *13* (7), 3911−3936.
(14) Song, Y.; Feng, X.; Lin, W. Metal-Organic Frameworks for Catalytic Applications.*Comp. Coord Chem.* **2021**, 228.
(15) He, C.; Si, D.-H.; Huang, Y.-B.; Cao, R. A CO2-Masked Carbene Functionalized Covalent Organic Framework for Highly Efficient Carbon Dioxide Conversion. *Angew. Chem., Int. Ed.* **2022**, *61* (40), e202207478.
(16) Feng, L.; Qiu, Y.; Guo, Q.-H.; Chen, Z.; Seale, J. S. W.; He, K.; Wu, H.; Feng, Y.; Farha, O. K.; Astumian, R. D.; Stoddart, J. F. Active mechanisorption driven by pumping cassettes. *Science* **2021**, *374* (6572), 1215−1221.
(17) Lin, R.-B.; Zhang, Z.; Chen, B. Achieving High Performance Metal−Organic Framework Materials through Pore Engineering. *Acc. Chem. Res.* **2021**, *54* (17), 3362−3376.
(18) Hendon, C. H.; Rieth, A. J.; Korzyński, M. D.; Dincă, M. Grand Challenges and Future Opportunities for Metal−Organic Frameworks. *ACS Central Science* **2017**, *3* (6), 554−563.
(19) Luo, Y.-C.; Chu, K.-L.; Shi, J.-Y.; Wu, D.-J.; Wang, X.-D.; Mayor, M.; Su, C.-Y. Heterogenization of Photochemical Molecular Devices: Embedding a Metal−Organic Cage into a ZIF-8-Derived Matrix To Promote Proton and Electron Transfer. *J. Am. Chem. Soc.* **2019**, *141* (33), 13057−13065.
(20) Wang, J.; Zhang, Y.; Zhang, P.; Hu, J.; Lin, R.-B.; Deng, Q.; Zeng, Z.; Xing, H.; Deng, S.; Chen, B. Optimizing Pore Space for Flexible-Robust Metal−Organic Framework to Boost Trace Acetylene Removal. *J. Am. Chem. Soc.* **2020**, *142* (21), 9744−9751.
(21) Cao, L.; Lin, Z.; Peng, F.; Wang, W.; Huang, R.; Wang, C.; Yan, J.; Liang, J.; Zhang, Z.; Zhang, T.; Long, L.; Sun, J.; Lin, W. Self-Supporting Metal−Organic Layers as Single-Site Solid Catalysts. *Angew. Chem., Int. Ed.* **2016**, *55* (16), 4962−4966.
(22) Lan, G.; Quan, Y.; Wang, M.; Nash, G. T.; You, E.; Song, Y.; Veroneau, S. S.; Jiang, X.; Lin, W. Metal−Organic Layers as Multifunctional Two-Dimensional Nanomaterials for Enhanced Photoredox Catalysis. *J. Am. Chem. Soc.* **2019**, *141* (40), 15767−15772.
(23) Feng, X.; Song, Y.; Lin, W. Dimensional Reduction of Lewis Acidic Metal−Organic Frameworks for Multicomponent Reactions. *J. Am. Chem. Soc.* **2021**, *143* (21), 8184−8192.
(24) Luo, T.; Fan, Y.; Mao, J.; Yuan, E.; You, E.; Xu, Z.; Lin, W. Dimensional Reduction Enhances Photodynamic Therapy of Metal−Organic Nanophotosensitizers. *J. Am. Chem. Soc.* **2022**, *144* (12), 5241−5246.
(25) Kalmutzki, M. J.; Hanikel, N.; Yaghi, O. M. Secondary building units as the turning point in the development of the reticular chemistry of MOFs. *Science Advances* **2018**, *4* (10), eaat9180.
(26) Quan, Y.; Lan, G.; Shi, W.; Xu, Z.; Fan, Y.; You, E.; Jiang, X.; Wang, C.; Lin, W. Metal−Organic Layers Hierarchically Integrate Three Synergistic Active Sites for Tandem Catalysis. *Angew. Chem., Int. Ed.* **2021**, *60* (6), 3115−3120.
(27) Quan, Y.; Lan, G.; Fan, Y.; Shi, W.; You, E.; Lin, W. Metal−Organic Layers for Synergistic Lewis Acid and Photoredox Catalysis. *J. Am. Chem. Soc.* **2020**, *142* (4), 1746−1751.
(28) Zheng, H.; Fan, Y.; Song, Y.; Chen, J. S.; You, E.; Labalme, S.; Lin, W. Site Isolation in Metal−Organic Layers Enhances Photoredox Gold Catalysis. *J. Am. Chem. Soc.* **2022**, *144* (24), 10694−10699.
(29) Drake, T.; Ji, P.; Lin, W. Site Isolation in Metal−Organic Frameworks Enables Novel Transition Metal Catalysis. *Acc. Chem. Res.* **2018**, *51* (9), 2129−2138.
(30) Konnerth, H.; Matsagar, B. M.; Chen, S. S.; Prechtl, M. H. G.; Shieh, F.-K.; Wu, K. C. W. Metal-organic framework (MOF)-derived catalysts for fine chemical production. *Coord. Chem. Rev.* **2020**, *416*, 213319.
(31) Lan, G.; Li, Z.; Veroneau, S. S.; Zhu, Y.-Y.; Xu, Z.; Wang, C.; Lin, W. Photosensitizing Metal−Organic Layers for Efficient Sunlight-Driven Carbon Dioxide Reduction. *J. Am. Chem. Soc.* **2018**, *140* (39), 12369−12373.
(32) Zhao, M.; Wang, Y.; Ma, Q.; Huang, Y.; Zhang, X.; Ping, J.; Zhang, Z.; Lu, Q.; Yu, Y.; Xu, H.; Zhao, Y.; Zhang, H. Ultrathin 2D Metal−Organic Framework Nanosheets. *Adv. Mater.* **2015**, *27* (45), 7372−7378.
(33) Jian, M.; Qiu, R.; Xia, Y.; Lu, J.; Chen, Y.; Gu, Q.; Liu, R.; Hu, C.; Qu, J.; Wang, H.; Zhang, X., Ultrathin water-stable metal-organic framework membranes for ion separation. *Science Advances* **2020**, *6* (23), eaay3998
(34) Wei, R.-J.; You, P.-Y.; Duan, H.; Xie, M.; Xia, R.-Q.; Chen, X.; Zhao, X.; Ning, G.-H.; Cooper, A. I.; Li, D., Ultrathin Metal−Organic

https://doi.org/10.1021/jacs.2c12599
J. Am. Chem. Soc. 2023, 145, 4158−4165

Framework Nanosheets Exhibiting Exceptional Catalytic Activity. *J. Am. Chem. Soc.* **2022**, *144*, 17487.
(35) Dong, J.; Mo, Q.; Wang, Y.; Jiang, L.; Zhang, L.; Su, C.-Y. Ultrathin Two-Dimensional Metal−Organic Framework Nanosheets Based on a Halogen-Substituted Porphyrin Ligand: Synthesis and Catalytic Application in CO2 Reductive Amination. *Eur. J. Chem.* **2022**, *28* (41), e202200555.
(36) Twilton, J.; Le, C.; Zhang, P.; Shaw, M. H.; Evans, R. W.; MacMillan, D. W. C. The merger of transition metal and photocatalysis. *Nat. Rev. Chem.* **2017**, *1* (7), 0052.
(37) Skubi, K. L.; Blum, T. R.; Yoon, T. P. Dual Catalysis Strategies in Photochemical Synthesis. *Chem. Rev.* **2016**, *116* (17), 10035−10074.
(38) Kojima, M.; Matsunaga, S. The Merger of Photoredox and Cobalt Catalysis. *Trends in Chemistry* **2020**, *2* (5), 410−426.
(39) Zhang, G.; Liu, C.; Yi, H.; Meng, Q.; Bian, C.; Chen, H.; Jian, J.-X.; Wu, L.-Z.; Lei, A. External Oxidant-Free Oxidative Cross-Coupling: A Photoredox Cobalt-Catalyzed Aromatic C−H Thiolation for Constructing C−S Bonds. *J. Am. Chem. Soc.* **2015**, *137* (29), 9273−9280.
(40) Cao, H.; Jiang, H.; Feng, H.; Kwan, J. M. C.; Liu, X.; Wu, J. Photo-induced Decarboxylative Heck-Type Coupling of Unactivated Aliphatic Acids and Terminal Alkenes in the Absence of Sacrificial Hydrogen Acceptors. *J. Am. Chem. Soc.* **2018**, *140* (47), 16360−16367.
(41) Zhao, H.; McMillan, A. J.; Constantin, T.; Mykura, R. C.; Juliá, F.; Leonori, D. Merging Halogen-Atom Transfer (XAT) and Cobalt Catalysis to Override E2-Selectivity in the Elimination of Alkyl Halides: A Mild Route toward contra-Thermodynamic Olefins. *J. Am. Chem. Soc.* **2021**, *143* (36), 14806−14813.
(42) Jia, Z.; Zhang, L.; Luo, S. Asymmetric C−H Dehydrogenative Allylic Alkylation by Ternary Photoredox-Cobalt-Chiral Primary Amine Catalysis under Visible Light. *J. Am. Chem. Soc.* **2022**, *144* (24), 10705−10710.
(43) Occhialini, G.; Palani, V.; Wendlandt, A. E. Catalytic, contra-Thermodynamic Positional Alkene Isomerization. *J. Am. Chem. Soc.* **2022**, *144* (1), 145−152.
(44) McManus, J. B.; Griffin, J. D.; White, A. R.; Nicewicz, D. A. Homobenzylic Oxygenation Enabled by Dual Organic Photoredox and Cobalt Catalysis. *J. Am. Chem. Soc.* **2020**, *142* (23), 10325−10330.
(45) Thullen, S. M.; Rovis, T. A Mild Hydroaminoalkylation of Conjugated Dienes Using a Unified Cobalt and Photoredox Catalytic System. *J. Am. Chem. Soc.* **2017**, *139* (43), 15504−15508.
(46) Wang, S.; Gao, Y.; Liu, Z.; Ren, D.; Sun, H.; Niu, L.; Yang, D.; Zhang, D.; Liang, X. a.; Shi, R.; Qi, X.; Lei, A. Site-selective amination towards tertiary aliphatic allylamines. *Nature Catalysis* **2022**, *5* (7), 642−651.
(47) Liu, W.-Q.; Lei, T.; Zhou, S.; Yang, X.-L.; Li, J.; Chen, B.; Sivaguru, J.; Tung, C.-H.; Wu, L.-Z. Cobaloxime Catalysis: Selective Synthesis of Alkenylphosphine Oxides under Visible Light. *J. Am. Chem. Soc.* **2019**, *141* (35), 13941−13947.
(48) Zhou, M.-J.; Zhang, L.; Liu, G.; Xu, C.; Huang, Z. Site-Selective Acceptorless Dehydrogenation of Aliphatics Enabled by Organo-photoredox/Cobalt Dual Catalysis. *J. Am. Chem. Soc.* **2021**, *143* (40), 16470−16485.
(49) Meng, Q.-Y.; Zhong, J.-J.; Liu, Q.; Gao, X.-W.; Zhang, H.-H.; Lei, T.; Li, Z.-J.; Feng, K.; Chen, B.; Tung, C.-H.; Wu, L.-Z. A Cascade Cross-Coupling Hydrogen Evolution Reaction by Visible Light Catalysis. *J. Am. Chem. Soc.* **2013**, *135* (51), 19052−19055.
(50) Dighe, S.; Juliá, F.; Luridiana, A.; Douglas, J. J.; Leonori, D. A photochemical dehydrogenative strategy for aniline synthesis. *Nature* **2020**, *584* (7819), 75−81.
(51) Constantin, T.; Zanini, M.; Regni, A.; Sheikh Nadeem, S.; Juliá, F.; Leonori, D. Aminoalkyl radicals as halogen-atom transfer agents for activation of alkyl and aryl halides. *Science* **2020**, *367* (6481), 1021−1026.
(52) Lan, G.; Ni, K.; Veroneau, S. S.; Luo, T.; You, E.; Lin, W. Nanoscale Metal−Organic Framework Hierarchically Combines High-Z Components for Multifarious Radio-Enhancement. *J. Am. Chem. Soc.* **2019**, *141* (17), 6859−6863.
(53) Zhao, W.; Sun, J. Triflimide (HNTf2) in Organic Synthesis. *Chem. Rev.* **2018**, *118* (20), 10349−10392.

https://doi.org/10.1021/jacs.2c12599
J. Am. Chem. Soc. 2023, 145, 4158−4165